IEEE Access
Multidisciplinary | Rapid Review | Open Access Journal

Received June 19, 2018, accepted July 19, 2018, date of publication August 7, 2018, date of current version August 28, 2018.

Digital Object Identifier 10.1109/ACCESS.2018.2862637

Port-Controlled Hamiltonian and Sliding Mode Control of Gantry Robot Based on Induction Motor Drives

BINGKUN ZHAO, HAISHENG YU, JINPENG YU, XUDONG LIU, AND HERONG WU
College of Automation and Electrical Engineering, Qingdao University, Qingdao 266071, China

Corresponding author: Haisheng Yu (yu.hs@163.com)

The work was supported in part by the Natural Science Foundation of China under Grant 61573203, Grant 61573204, and Grant 61703222, and in part by the Shandong Province Outstanding Youth Fund under Grant ZR2015JL022.

ABSTRACT A port-controlled Hamiltonian (PCH) control approach is presented to solve the position tracking problem of gantry robot based on induction motor (IM) drives. First, a robot model is established. Second, a PCH controller is designed to realize accurate position tracking of a gantry robot. For IM drives, it is convenient to choose a direct torque control strategy based on the sliding mode control, which overcomes the higher ripples of torque and flux. Third, a voltage reconstruction technique is introduced to calculate the stator voltage of the IM, which replaces the stator voltage measurement of the IM. Finally, the load torque observer is developed to estimate an unknown load torque. The asymptotic stability of the robot system is proved by the Lyapunov stability theory. Simulation results indicate that the system has excellent position tracking performances and load disturbance attenuation ability.

INDEX TERMS Gantry robot, port-controlled Hamiltonian, induction motor, sliding mode control, load torque observer.

I. INTRODUCTION

The gantry robot is widely used in industry applications. The techniques of robots control are well treated in the literature, such as back-stepping control [1], adaptive Neuro-sliding mode control [2]. The back-stepping controller generates the desired control force on the mechanical subsystem. The adaptive Neuro-sliding mode control method has a good steady tracking accuracy without chattering in the control signal. The position tracking issues of the robots are increasingly being concerned [3], [4]. Some simple methods are emploied to position control of robots, such as gravity compensation [5] and proportion differentiation (PD) control [6]. While the fixed parameters of PD control can not adapt the variability of system. Sometimes robot manipulators are difficult to establish an accurate mathematical model due to robot's uncertainties and nonlinear characteristics [7]. For this reason, a large number of intelligent control strategies are applied to the gantry robot drive systems. For instance, adaptive neural network [8], [9], adaptive fuzzy neural network [10], and RBF neural network [11]. But the intelligent control relies on numerous programming languages that are complex and cumbersome. Note that the Port-Controlled Hamiltonian (PCH) control has attracted lots of attentions and is widely applied to the nonlinear systems [12], [13]. The dynamics model of gantry robot can also be viewed as a PCH system and then the PCH controller can be obtained by damping injection and energy-shaping [14], [15]. So the PCH controller is designed to realize accurate position tracking of gantry robot.

For the drive systems of gantry robot, the induction motor (IM) is broadly used in servo systems since it has the advantages of low price and ruggedness. Therefore, the IM is suitable for the application in the robot. Field oriented control (FOC) and direct torque control (DTC), appear to be very convenient for good dynamic response. The DTC strategy based on hysteresis controllers and lookup switching table has more advantages such as fast response and less dependence to the parameters of IM. However, the main problems of DTC are the high torque and flux ripples, as well as the variable switch frequency, which increase control difficulty in low speed regions [16], [17]. Nowadays, there are different approaches being used to cope with these disadvantages. In [18], a multilevel converter is provided to reduce the ripples. Nevertheless, the number of power switches is increased which causes the lower efficiency of the control system.

The model predictive control (MPC) also has the ability to determine a suitable voltage vector which can reduce the ripples [19]. Nevertheless, the high complexity of the control law is the main drawback of MPC. For IM drives, it is convenient to choose direct torque control (DTC) strategy based on the sliding mode control (SMC), which overcomes the higher ripples of torque and flux, as well as the variable switch frequency. The sliding mode control (SMC) has good robustness and fast response, thus it can be designed to control the torque and flux of IM. According to [20] and [21], the torque and flux sliding mode controllers are developed to reduce the ripples. Then, a sliding mode direct torque control (SM-DTC) strategy is presented to the control of the IM. The robot control combined with motor control is closer to the actual industry application. And the torque is the connection between the robot and induction motors. At the same time, the desired torque obtained from PCH controller can be the input of induction motors directly instead of the torque current conversion in vector control. The contributions of the article are:

(1) The PCH control scheme is developed to enhance the position tracking performance of gantry robot.

(2) Compared with [22] and [23], a novel DTC strategy based on the sliding mode control is investigated which decreases the torque and flux ripples. At the same time, a voltage reconstruction technique is proposed to calculate the stator voltage, which replaces the stator voltage measurement of the IM.

(3) The robot system has good load disturbance attenuation performance by introducing the load torque observer.

(4) The robot control combined with motor control is closer to the actual industry application. The whole system is asymptotically stable based on Lyapunov stability theory.

II. MODEL OF GANTRY ROBOT SYSTEM

A. KINEMATICS AND DYNAMICS MODELS OF GANTRY ROBOT

The gantry robot has three axes, where x, y axis are in the horizontal plane, and z axis is vertical to the horizontal level. Three axes are perpendicular to eath other. The IM is chosen as the drive motor. The robot model is shown in Fig.1 and base coordinate system is set at point 'o'.

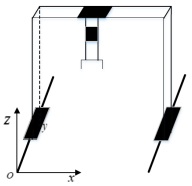

FIGURE 1. The model of gantry robot.

The kinematics model can be presented as

$$\begin{bmatrix} x \\ y \\ z \end{bmatrix} = \begin{bmatrix} d_x/2\pi & 0 & 0 \\ 0 & d_y/2\pi & 0 \\ 0 & 0 & d_z/2\pi \end{bmatrix} \begin{bmatrix} q_x \\ q_y \\ q_z \end{bmatrix} \tag{1}$$

where $q = \begin{bmatrix} q_x & q_y & q_z \end{bmatrix}^T$, d_i are the angular position and gear rotation radius of load shaft, respectively, $i = x, y, z$.

The drive structure of i-axis is shown in Fig.2.

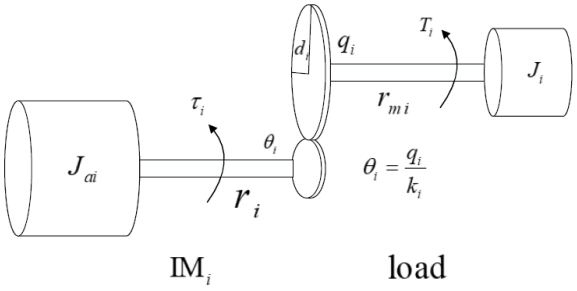

FIGURE 2. The drive structure of i-axis.

where $i = x, y, z$, J_{ai}, J_i are the inertia moments of motor and load, respectively. τ_i, T_i are the torque of motor and load, respectively. θ_i, q_i are angular positions of motor and load, respectively. r_i, r_{mi} are the friction coefficients of motor and load, respectively. k_i is the reduction ratio between motor and load. Thus, the dynamics equation of i-axis between motor and load is calculated as follows

$$(J_{ai} + J_i k_i^2)\ddot{\theta}_i + (r_i + r_{mi} k_i^2)\dot{\theta}_i = \tau_i. \tag{2}$$

The robot dynamics model can be described as

$$M(\theta)\ddot{\theta} + C(\theta, \dot{\theta})\dot{\theta} + R_f\dot{\theta} + G = \tau \tag{3}$$

where $\theta, \dot{\theta}, \ddot{\theta}$ are 3×1 angular position, velocity and acceleration vectors, respectively, $M(\theta)$ is a 3×3 positive definite and symmetric mixed inertia matrix, G is a 3×1 gravity torque vector, τ represents a 3×1 input torque and $\tau = \begin{bmatrix} \tau_x & \tau_y & \tau_z \end{bmatrix}^T$, R_f is friction coefficient, $C(\theta, \dot{\theta})$ is a 3×1 matrix of centripetal and Coriolis forces.

$$\begin{aligned} M(\theta) &= diag\left\{J_{ax} + J_x k_x^2, J_{ay} + J_y k_y^2, J_{az} + J_z k_z^2\right\}, \\ R_f &= \begin{bmatrix} r_x + r_{mx} k_x^2 & r_y + r_{my} k_y^2 & r_z + r_{mz} k_z^2 \end{bmatrix}^T, \\ G &= \begin{bmatrix} 0 & 0 & m_z g k_z d_z/(2\pi) \end{bmatrix}^T, \quad C(\theta, \dot{\theta}) = 0. \end{aligned}$$

B. THE MATHEMATICAL MODEL OF THE IM

The model of the IM can be expressed in $\alpha\beta$ frame. It is expressed as [24]

$$\begin{cases} \dot{i}_{s\alpha i} = -\dfrac{R_{si}L_{ri} + R_{ri}L_{si}}{\sigma L_{si}L_{ri}} i_{s\alpha i} - \omega_{ri} i_{s\beta i} + \dfrac{R_{ri}\lambda_{s\alpha i}}{\sigma L_{si}L_{ri}} + \\ \dfrac{\omega_{ri}\lambda_{s\beta i}}{\sigma L_{ri}} + \dfrac{u_{s\alpha i}}{\sigma L_{si}} \\ \dot{i}_{s\beta i} = -\dfrac{R_{si}L_{ri} + R_{ri}L_{si}}{\sigma L_{si}L_{ri}} i_{s\beta i} + \omega_{ri} i_{s\alpha i} + \dfrac{R_{ri}\lambda_{s\beta i}}{\sigma L_{si}L_{ri}} - \\ \dfrac{\omega_{ri}}{\sigma L_{ri}} + \dfrac{u_{s\beta i}}{\sigma L_{si}} \\ \dot{\lambda}_{s\alpha i} = u_{s\alpha i} - R_{si} i_{s\alpha i} \\ \dot{\lambda}_{s\beta i} = u_{s\beta i} - R_{si} i_{s\beta i} \\ \dot{\omega}_i = \dfrac{\tau_i}{J_i} - \dfrac{\tau_{Li}}{J_i} \\ \dot{\theta}_i = \omega_i \end{cases} \tag{4}$$

where $i_{s\alpha i}$, $i_{s\beta i}$ are stator current components, respectively, $\lambda_{s\alpha i}$, $\lambda_{s\beta i}$ are stator flux components, respectively, R_{si}, R_{ri} are stator and rotor resistances, respectively, L_{si}, L_{ri} are stator and rotor inductances, respectively, $\sigma = 1 - \frac{L_{mi}^2}{L_{si}L_{ri}}$ is Blondel's coefficient, L_{mi} is the mutual statorrotor inductance, J_i is inertia moment, θ_i, ω_i are the angular position and velocity, respectively. The i is a subscript and $i = x, y, z$.

The electromagnetic torque can be presented as

$$\tau_i = n_p(\lambda_{s\alpha i} i_{s\beta i} - \lambda_{s\beta i} i_{s\alpha i}) \tag{5}$$

$$q_i = k_i \theta_i \tag{6}$$

where n_p is the number of pole pairs.

III. CONTROLLER DESIGN

A. GANTRY ROBOT CONTROL SYSTEM

According to inverse kinematics and dynamics model of robot, the whole servo control system of robot is shown in Fig.3. λ_{sx}^*, λ_{sy}^* and λ_{sz}^* are the constant fluxes reference (0.8Wb). After the desired position (x^*, y^*, z^*) is given, the reference angle position (q_x^*, q_y^*, q_z^*) of robot is obtained by inverse kinematics. Then the reference torque τ_x^*, τ_y^* and τ_z^* can be calculated by PCH controller which is designed based on position errors. Finally, the SMC strategy based on torque and flux errors is developed to motor control subsystems.

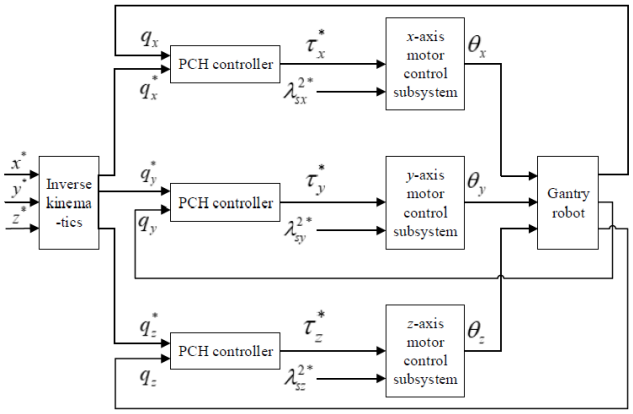

FIGURE 3. Gantry robot control system schematic diagram.

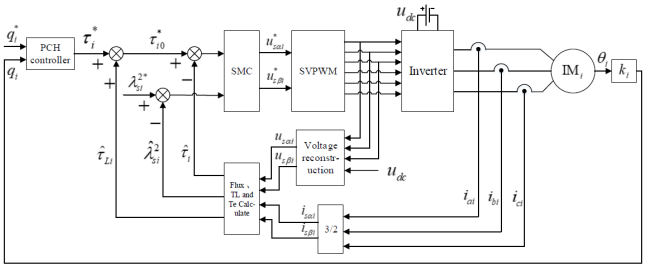

FIGURE 4. The DTC of IM based on SMC.

B. THE I-AXIS CONTROL SYSTEM

The i-axis control system of the robot is expressed in Fig.4. On the one hand, the SMC is designed as inner loop controller to decrease the ripples of torque and flux. On the other hand, a PCH controller is applied as position regudation. What's more, a load torque obsever is added to τ_i^* and then $\tau_{i0}^* = \tau_i^* + \hat{\tau}_{Li}$.

C. PCH CONTROLLER DESIGN

To improve the position tracking performance, the PCH control strategy is introduced. Then the energy shaping and damping injection methods are proposed to obtain the torque for the IM.

Define $p = M(\theta)\dot{\theta}$ as system momenta, $\eta = \begin{bmatrix} \theta & p \end{bmatrix}^T$ as the state vector, then $\dot{\theta} = M^{-1}(\theta)p$ and $V(\eta) = m_z g k_z d_z \theta_z/(2\pi)$. The Hamiltonian system of the robot is expressed as

$$H(\eta) = \frac{1}{2}\eta^T M^{-1}(\theta)\eta + V(\eta). \tag{7}$$

The Hamiltonian system of gantry robot is shown in the following [25]

$$\dot{\eta} = (J - R)\frac{\partial H(\eta)}{\partial \eta} + g(\eta)\tau \tag{8}$$

where R represents the dissipation, the interconnection structure is captured in matrix $g(\eta)$ and the skew-symmetricmatrix $J = -J^T$.

$$J = -J^T = \begin{bmatrix} 0 & I \\ -I & 0 \end{bmatrix}, \quad R = \begin{bmatrix} 0 & 0 \\ 0 & R_f \end{bmatrix}, \quad g(\eta) = \begin{bmatrix} 0 & I \end{bmatrix}^T.$$

Let the desired Hamiltonian function of robot system as follows

$$H_d(\eta) = \frac{1}{2}(\eta - \eta^*)^T M_d^{-1}(\theta)(\eta - \eta^*) + \frac{1}{2}\rho(\eta - \eta^*)^2 \tag{9}$$

where, $M(\theta) = M_d(\theta) = M_d^T(\theta) > 0$, and $V_d(\eta - \eta^*) = \frac{1}{2}\rho(\eta - \eta^*)^2$ represents the potential energy function, $\rho(> 0)$ is a parameter. Thus $V_d(\eta - \eta^*)$ has an minimum at the desired equilibrium point $\eta^* = \begin{bmatrix} \theta^* & 0 \end{bmatrix}^T$

$$\theta^* = \arg\min V_d(\eta - \eta^*). \tag{10}$$

The desired closed-loop Hamiltonian system can be described as

$$\dot{\eta} = (J_d - R_d)\frac{\partial H_d(\eta)}{\partial \eta} \tag{11}$$

where, K_v is the designed parameter, the desired interconnection matrix and damping matrix are

$$J_d = -J_d^T = \begin{bmatrix} 0 & I \\ -I & 0 \end{bmatrix}, \quad R_d = R_d^T = \begin{bmatrix} 0 & 0 \\ 0 & K_v \end{bmatrix} \geq 0.$$

The PCH position controller is obtained from Eq.(8) and Eq.(11), that is

$$(J - R)\frac{\partial H(\eta)}{\partial \eta} + g(\eta)\tau = (J_d - R_d)\frac{\partial H_d(\eta)}{\partial \eta}$$

$$\tau^* = \left[\frac{\partial H(\eta)}{\partial \theta} + R_f\frac{\partial H(\eta)}{\partial p} - \frac{\partial H_d(\eta)}{\partial \theta} - K_v\frac{\partial H_d(\eta)}{\partial p}\right] \tag{12}$$

therefore, τ_x^*, τ_y^* and τ_z^* can be calculated as follows

$$\begin{cases} \tau_x^* = (r_x + r_m k_i^2)\dot{\theta}_x - \rho(\theta_x^* - \theta_x) - \dfrac{K_v p_x}{(J_{ax} + J_x)k_i^2} \\ \tau_y^* = (r_y + r_m k_i^2)\dot{\theta}_y - \rho(\theta_y^* - \theta_y) - \dfrac{K_v p_y}{(J_{ay} + J_y)k_i^2} \\ \tau_z^* = \dfrac{m_z g k d_z}{2\pi} + (r_z + r_m k_i^2)\dot{\theta}_z - \rho(\theta_z^* - \theta_z) - \dfrac{K_v p_z}{(J_{az} + J_z)k_i^2} \end{cases}$$
$$q_i^* = k_i\theta_i^*, \quad q_i = k_i\theta_i, \ i = x, y, z.$$

Define $V_1 = H_d\ (\eta)$ as the Lyapunov function, the derivative of V_1 along trajectories of Eq.(11) can be written as follows

$$\begin{aligned} \dot{V}_1 &= \left(\frac{\partial H_d(\eta)}{\partial \eta}\right)^T \dot{\eta} = -\left(\frac{\partial H_d(\eta)}{\partial \eta}\right)^T (J_d - R_d)\left(\frac{\partial H_d(\eta)}{\partial \eta}\right) \\ &= -\left(\frac{\partial H_d(\eta)}{\partial \eta}\right)^T R_d \left(\frac{\partial H_d(\eta)}{\partial \eta}\right) \le 0. \end{aligned} \tag{13}$$

if $\eta = \eta^*$, then $\frac{\partial H_d\ (\eta)}{\partial \eta} = 0$ and $\frac{\partial^2 H_d\ (\eta)}{\partial \eta^2} \ge 0$. According to LaSalle's invariance set principle, when $\left\{\eta \in R^n \left| \left(\frac{\partial H_d\ (\eta)}{\partial \eta}\right)^T R_d \left(\frac{\partial H_d\ (\eta)}{\partial \eta}\right) = 0 \right.\right\}$, the PCH position subsystem is asymptotically stable at the desired equilibrium point η^*.

D. LOAD TORQUE OBSERVER DESIGN

In order to estimate the unknown load torque, the load torque observer is developed [26] ,[27].

When the load torque is known and constant, from Eq.(4) we get

$$\begin{cases} \dot{\theta}_i = \omega_i \\ \dot{\omega}_i = \dfrac{\tau_i}{J_i} - \frac{\tau_{Li}}{J_i} \\ \dot{\tau}_{Li} = 0 \end{cases} \tag{14}$$

However, the load torque is uncertain in actual industry applications. Thus, a load torque observer equation is designed as

$$\begin{cases} \dot{\hat{\theta}}_i &= \omega_i + k_{1i}(\theta_i - \hat{\theta}_i) \\ \dot{\hat{\omega}}_i &= \dfrac{\tau_i}{J_i} - \frac{\hat{\tau}_{Li}}{J_i} + k_{2i}(\theta_i - \hat{\theta}_i) \\ \dot{\hat{\tau}}_{Li} &= k_{3i}(\theta_i - \hat{\theta}_i) \end{cases} \tag{15}$$

where, k_{1i}, k_{2i}, k_{3i} are designed parameters. Define $\tilde{\theta}_i = \theta_i - \hat{\theta}_i$, $\tilde{\omega}_i = \omega_i - \hat{\omega}_i$, $\tilde{\tau}_{Li} = \tau_{Li} - \hat{\tau}_{Li}$ and $w = \left[\tilde{\theta}_i\ \tilde{\omega}_i\ \tilde{\tau}_{Li}\right]^T$ as the estimated errors and state error vector, respectively. The error equation of observer has the form

$$\dot{w} = Aw \tag{16}$$

where

$$A = \begin{bmatrix} -k_{1i} & 1 & 0 \\ -k_{2i} & 0 & -\frac{1}{J_i} \\ -k_{3i} & 0 & 0 \end{bmatrix}$$

The positive Lyapunov function can be indicated in the following

$$V_2 = w^T P w \tag{17}$$

where P is a positive definite matrix. By the Lyapunov equation $A^T P + PA = -Q$ ($Q = diag\left\{1\ 1\ 1\right\}$), P can be calculated as follows

$$P = \begin{bmatrix} \dfrac{J_i k_{2i}}{2k_{3i} + 2k_{1i}k_{2i}J_i} & 0 & \dfrac{1}{2k_{3i} + 2k_{1i}k_{2i}J_i} \\ 0 & \dfrac{J_i}{2k_{3i} + 2k_{1i}k_{2i}J_i} & 0 \\ \dfrac{1}{2k_{3i} + 2k_{1i}k_{2i}J_i} & 0 & \dfrac{-k_1}{(2k_{3i} + 2k_{1i}k_{2i}J_i)k_{3i}} \end{bmatrix}$$

we can get $k_{1i} > -\frac{k_{3i}}{k_{2i}J_i}, k_{2i} > 0, k_{3i} < 0$ by judging $|P|_{11} > 0, |P|_{22} > 0, |P|_{33} > 0$ so that P is a positive definite matrix. Therefore, we have

$$\dot{V}_2 < 0. \tag{18}$$

According to the Lyapunov stability theorem, the load torque observer subsystem can be asymptotically stable. Thus when τ_{Li} is unknown, $\hat{\tau}_{Li}$ can replace τ_{Li}. The characteristic equation of Eq.(16) is given as

$$s^3 + k_{1i}s^2 + k_{2i}s - k_{3i}/J_i = 0. \tag{19}$$

All the poles of the observer are set to be $s_1 = s_2 = s_3 = s_p\ (< 0)$ by selection of parameters as

$$k_{1i} = -3s_p, \quad k_{2i} = 3s_p^2, \quad k_{3i} = J_i s_p^3.$$

E. VOLTAGE RECONSTRUCTION

The stator voltage reconstruction strategy based on DC voltage and inverter switch signal is proposed [28], which replaces the stator voltage measurement of the IM. In Fig.5, the state of each switch in the inverter is shown by $s_1, s_2, s_3, s_4, s_5, s_6$ and u_{dc} is measurable. When the upper bridge switch is turned on, s_1=1 (or s_2, s_3), the lower bridge switch is turned on, s_1=0 (or s_2, s_3), therefore the two switches of the same bridge are on alternatively. Then, applying SVPWM signal transformation principle, we can get six pulses which are used to control the power converter to provide the desired three-phase voltages. The different instantaneous values u_a, u_b, u_c can be obtained by selecting different switch variables s_1, s_2 and s_3.

The state average model of the inverter is showed as

$$\begin{cases} u_a = \dfrac{u_{dc}}{3}(2s_1 - s_2 - s_3) \\ u_b = \dfrac{u_{dc}}{3}(2s_2 - s_1 - s_3) \\ u_c = \dfrac{u_{dc}}{3}(2s_3 - s_1 - s_2) \end{cases} \tag{20}$$

The stator voltage in $\alpha\beta$ frame is

$$\begin{bmatrix} u_{s\alpha} \\ u_{s\beta} \end{bmatrix} = \sqrt{\frac{2}{3}} \begin{bmatrix} 1 & -\frac{1}{2} & -\frac{1}{2} \\ 0 & \frac{\sqrt{3}}{2} & -\frac{\sqrt{3}}{2} \end{bmatrix} \begin{bmatrix} u_a \\ u_b \\ u_c \end{bmatrix}. \tag{21}$$

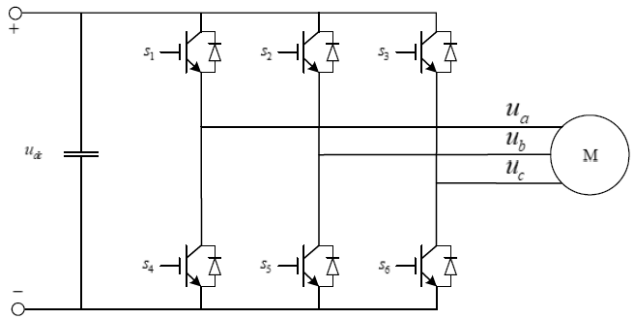

FIGURE 5. Inverter and motor block diagram.

The reconstructed stator voltage can be calculated by Eq.(21). The stator flux amplitude and phase angle are calculated as follows

$$\begin{cases} \lambda_{s\alpha i} = \int (u_{s\alpha i} - R_{si} i_{s\alpha i}) dt \\ \lambda_{s\beta i} = \int (u_{s\beta i} - R_{si} i_{s\beta i}) dt \\ \hat{\lambda}_{si}^2 = \lambda_{s\alpha i}^2 + \lambda_{s\beta i}^2 \\ \varphi = \arctan(\lambda_{s\beta i} / \lambda_{s\alpha i}). \end{cases} \tag{22}$$

The estimated electromagnetic torque is given as

$$\hat{\tau}_i = n_p(\lambda_{s\alpha i} i_{s\beta i} - \lambda_{s\beta i} i_{s\alpha i}). \tag{23}$$

F. SMC DESIGN

To simplify the design of the SMC controllers [29], [30], the errors of the torque and flux are taken as their sliding surfaces, respectively.

$$s_{1i} = e_{1i} = \tau_{i0}^* - \hat{\tau}_i \tag{24}$$

$$s_{2i} = e_{2i} = \lambda_{si}^{2*} - \hat{\lambda}_{si}^2 \tag{25}$$

the derivatives of Eq.(24) and Eq.(25) are expressed as follows

$$\begin{aligned} \dot{s}_{1i} &= \dot{\tau}_{i0}^* - n_{pi}[\dot{\lambda}_{s\alpha i} i_{s\beta i} + \lambda_{s\alpha i} \dot{i}_{s\beta i} - \dot{\lambda}_{s\beta i} i_{s\alpha i} - \lambda_{s\beta i} \dot{i}_{s\alpha i}] \\ &= \dot{\tau}_{i0}^* - n_{pi}[A + \omega_{ri}(i_{s\alpha i}\lambda_{s\alpha i} + i_{s\beta i}\lambda_{s\beta i}) \\ &\quad + \frac{R_{si}L_{ri} + R_{ri}L_{si}}{\sigma L_{si} L_{ri}}(i_{s\alpha i}\lambda_{s\beta i} - i_{s\beta i}\lambda_{s\alpha i}) - \frac{\omega_{ri}}{\sigma L_{si}}\lambda_{si}^2] \end{aligned} \tag{26}$$

$$\dot{s}_{2i} = \dot{\lambda}_{si}^{2*} - \dot{\lambda}_{si}^2 = \dot{\lambda}_{si}^{2*} - 2B + 2R_{si}(i_{s\alpha i}\lambda_{s\alpha i} - i_{s\beta i}\lambda_{s\beta i}) \tag{27}$$

where

$$\begin{aligned} A &= (i_{s\beta i} - \frac{\lambda_{s\beta i}}{\sigma L_{si}})u_{s\alpha i} + (\frac{\lambda_{s\alpha i}}{\sigma L_{si}} - i_{s\alpha i})u_{s\beta i}, \\ B &= u_{s\alpha i}\lambda_{s\alpha i} + u_{s\beta i}\lambda_{s\beta i}. \end{aligned}$$

The exponential reaching laws of sliding mode controller are designed as

$$\dot{s}_{1i} = -c_{1i}s_{1i} - \varepsilon_{1i} sgn(s_{1i}) \tag{28}$$

$$\dot{s}_{2i} = -c_{2i}s_{2i} - \varepsilon_{2i} sgn(s_{2i}) \tag{29}$$

where $c_{1i}, \varepsilon_{1i}, c_{2i}, \varepsilon_{2i} > 0$.

According Eq.(26), Eq.(27), Eq.(28) and Eq.(29), the value of A, B can be calculated below

$$\begin{aligned} A = &\frac{c_{1i}s_{1i} + \varepsilon_{1i} sgn(s_{1i}) + \dot{\tau}_i^*}{n_p} - \omega_{ri}(i_{s\alpha i}\lambda_{s\alpha i} + i_{s\beta i}\lambda_{s\beta i}) \\ &- \frac{R_{si}L_{ri} + R_{ri}L_{si}}{\sigma L_{si}L_{ri}}(i_{s\alpha i}\lambda_{s\beta i} - i_{s\beta i}\lambda_{s\alpha i}) + \frac{\omega_{ri}}{\sigma L_{si}}\lambda_{si}^2, \end{aligned} \tag{30}$$

$$B = \frac{c_{2i}s_{2i} + \varepsilon_{2i} sgn(s_{2i}) + \dot{\lambda}_{si}^{2*}}{2} + R_{si}(i_{s\alpha i}\lambda_{s\alpha i} - i_{s\beta i}\lambda_{s\beta i}). \tag{31}$$

The sliding mode controller can be calculated by Eq.(30) and Eq.(31)

$$u_{s\alpha i}^* = \frac{\sigma L_{si}\lambda_{s\beta i}A - (\lambda_{s\alpha i} - \sigma L_{si} i_{s\alpha i})B}{\sigma L_{si}(i_{s\beta i}\lambda_{s\beta i} - i_{s\alpha i}\lambda_{s\alpha i}) - \lambda_{si}^2}, \tag{32}$$

$$u_{s\beta i}^* = \frac{\sigma L_{si}\lambda_{s\alpha i}A - (\sigma L_{si} i_{s\beta i} - \lambda_{s\beta i})B}{\lambda_{si}^2 - \sigma L_{si}(i_{s\alpha i}\lambda_{s\alpha i} + i_{s\beta i}\lambda_{s\beta i})}. \tag{33}$$

To prove the asymptotic stability of the sliding mode subsystem, define $s = [\, s_{1i}\ s_{2i}\,]^T$ as the state vector and let $V_3 = \frac{1}{2}s^T s$ be the Lyapunov function. Therefore the derivative of V_3 is calculated in the following

$$\begin{aligned} \dot{V}_3 = s^T\dot{s} &= -[\, s_{1i}\ s_{2i}\,]\begin{bmatrix} c_{1i}s_{1i} + \varepsilon_{1i} sgn(s_{1i}) \\ c_{2i}s_{2i} + \varepsilon_{2i} sgn(s_{2i}) \end{bmatrix} \\ &= -c_{1i}s_{1i}^2 - \varepsilon_{1i} sgn(s_{1i})s_{1i} - c_{2i}s_{2i}^2 - \varepsilon_{2i} sgn(s_{2i})s_{2i} \\ &< -c_{1i}s_{1i}^2 - \varepsilon_{1i}\,|s_{1i}| - c_{2i}s_{2i}^2 - \varepsilon_{2i}\,|s_{2i}| < 0 \end{aligned} \tag{34}$$

if and only if $s_{1i} = s_{2i} = 0$, $\dot{V}_3 = 0$, thus the sliding mode subsystem is asymptotically stable.

G. STABILITY ANALYSIS

The Lyapunov function of whole system is chosen as V, and $V = V_1 + V_2 + V_3$. According to Eq.(13), Eq.(18), Eq.(34), and based on the Lyapunov stability theory, then $V > 0$, $\dot{V} < 0$, thus the whole system is asymptotically stable.

IV. SIMULATION RESULTS

The simulations are carried out with the following parameters of induction motor and robot: $R_s = 0.96419\Omega$, $R_r = 0.93766\Omega$, $L_r = 6.43858$mH, $L_s = 6.08925$mH, $n_p = 2$, $L_m = 5.9$mH, $P_n = 1.5$KW, $U_n = 220$V, and $m_i = 1$kg, $r_i = 0.01$, $r_{mi} = 0.1$, $J_{ai} = 0.03kg.m^2$, $J_i = 0.1kg.m^2$, $d_i = 0.5$cm, $k_i = 10$ and the robot operating space is $(3\times3\times3)$m. The parameters of PCH and SMC controllers are $K_v = 2$, $\rho = 2$,$c_{1i} = 40000$, $c_{2i} = 3000$, $\varepsilon_{1i} = 1$, $\varepsilon_{2i} = 1$. The parameters of PD control are $K_p = 40$, $K_D = 3$.

Case 1: The (0,0,0) and (1m, 1.2m, 1.4m) are initial and desired positions, respectively. In this case, 2N.m load torque is inserted at t=0s and then 10N.m load torque is added at t=2s. Fig.6 to Fig.15 give the position tracking performance of robot and the responses of the IM. It can be seen from Fig.6 and Fig.7 that the proposed PCH and SMC methods have better position tracking performance. Moreover, Fig.8 and Fig.9 show the speed responses of robot. It is obvious that PCH and SMC can keep better speed responses

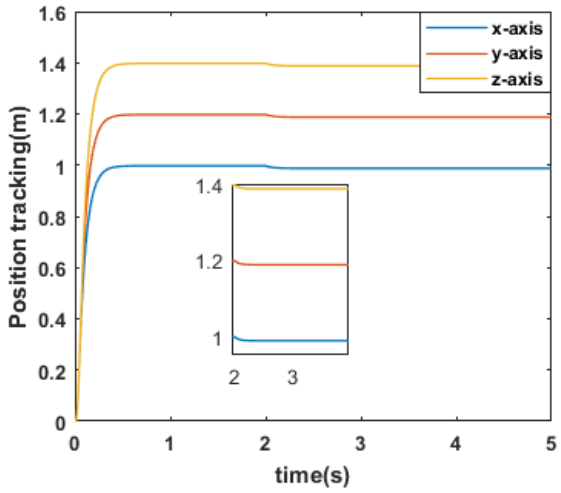

FIGURE 6. Position curves of PD and hysteresis control.

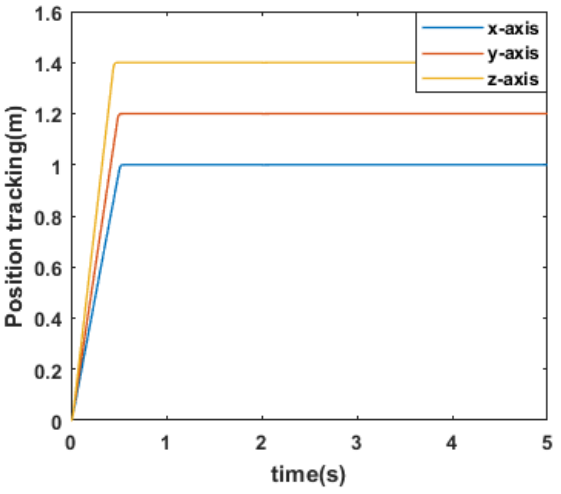

FIGURE 7. Position curves of PCH and SMC control.

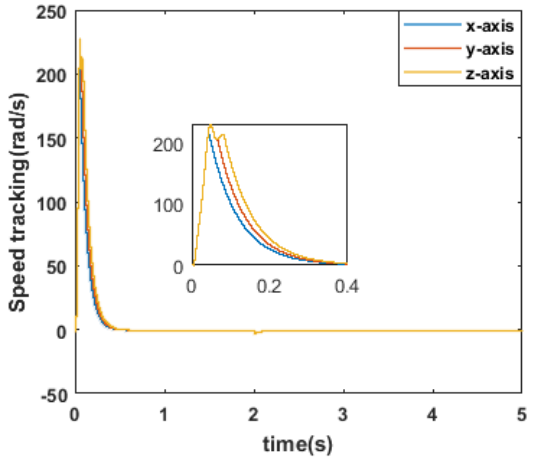

FIGURE 8. Speed curves of PD and hysteresis control.

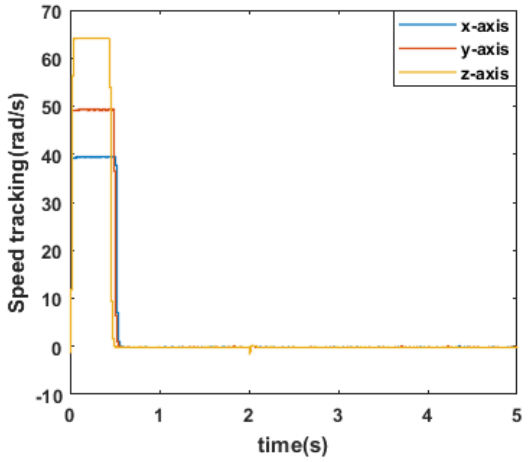

FIGURE 9. Speed curves of PCH and SMC control.

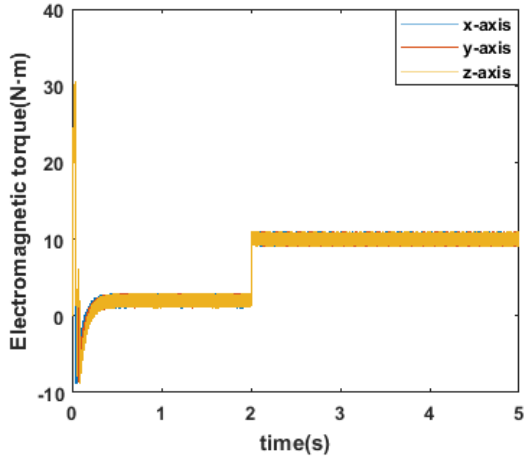

FIGURE 10. Electromagnetic torque curves of PD and hysteresis control.

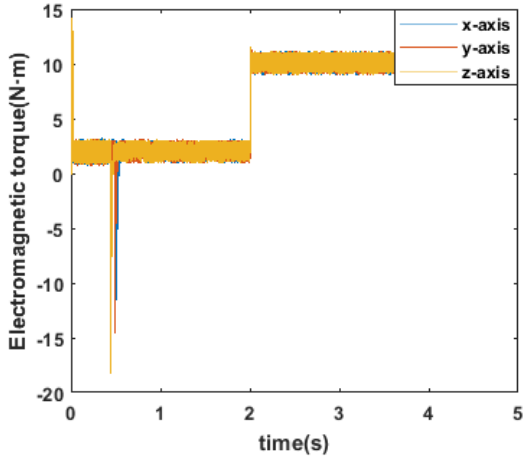

FIGURE 11. Electromagnetic torque curves of PCH and SMC control.

than PD control. From Fig.11, we can know that the proposed PCH and SMC controllers have good torque dynamics. The stator flux has better performance than traditional hysteresis control via Fig.12 when the IM moves with a constant velocity. Fig.13 presents that the reconstructed stator voltage can replace the measured stator voltage. At t=2s, different *sp*

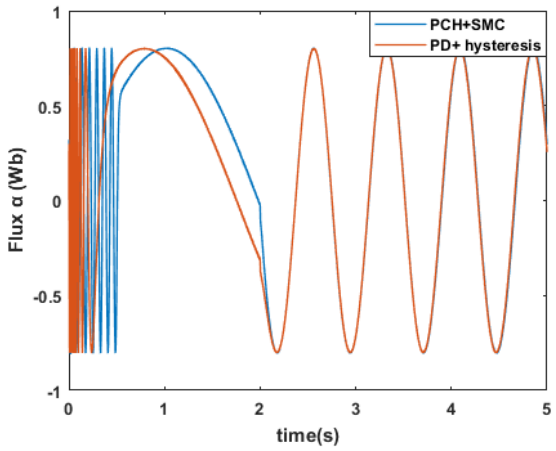

FIGURE 12. Flux α curves.

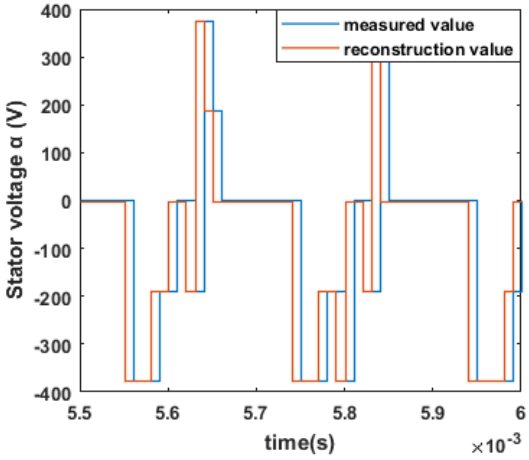

FIGURE 13. Voltage reconstruction curves.

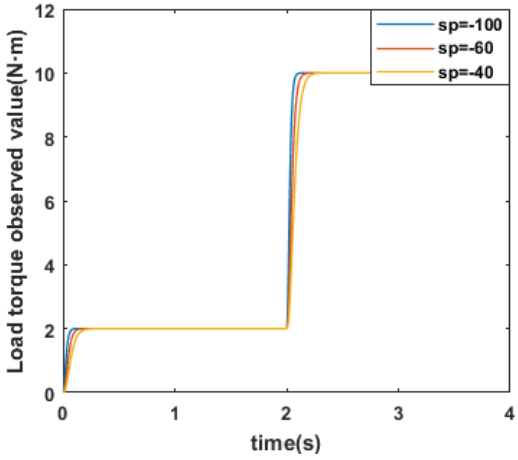

FIGURE 14. Load torque observation curve.

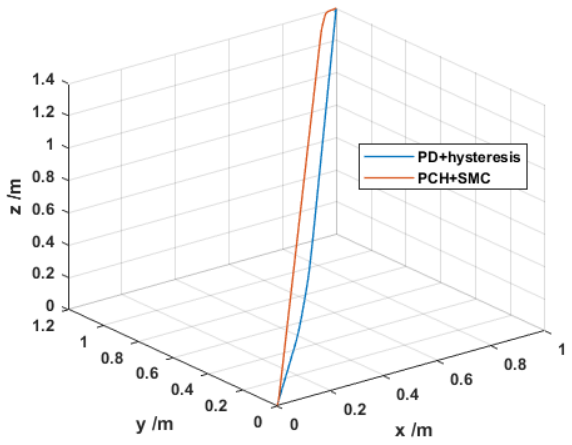

FIGURE 15. Space motion trajectory.

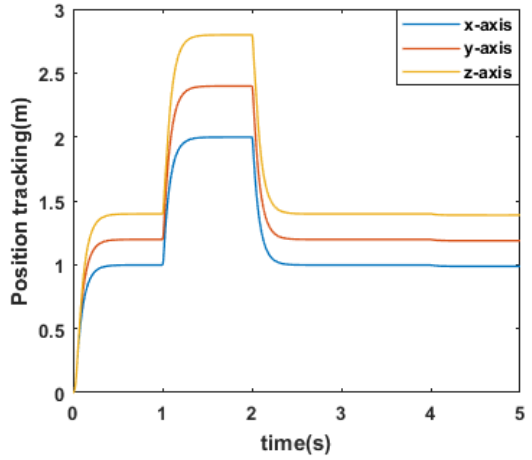

FIGURE 16. Position curves of PD and hysteresis control.

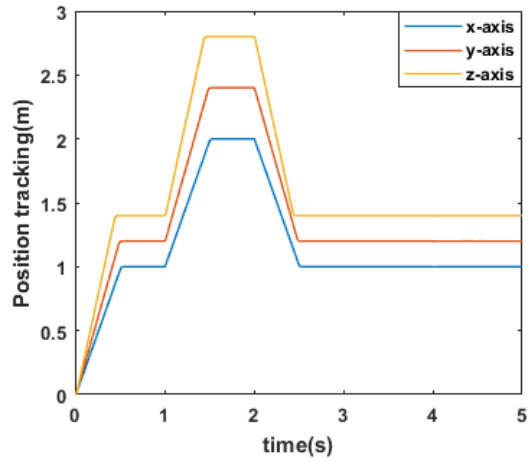

FIGURE 17. Position curves of PCH and SMC control.

values ($sp = -100, sp = -60, sp = -40$) are added to the load torque observation, Fig.14 illustrates that there is a better unknown load torque tracking performance when $sp = -100$. Finally, Fig.15 show that the PCH and SMC strategies have smoother trajectories than classical PD and hysteresis control.

Case 2: A trapezoidal position signal is applied to the robot. Before t=1s the space position is (1m, 1.2m, 1.4m),

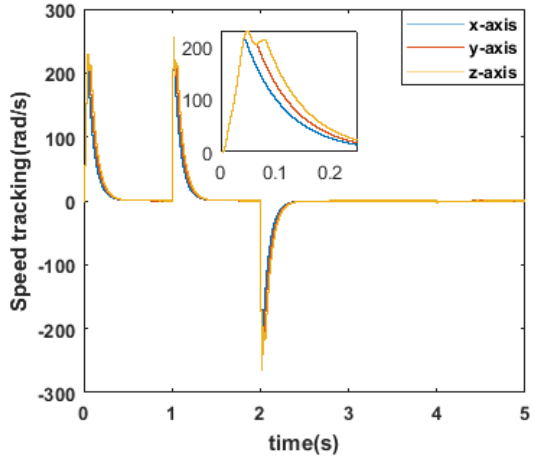

FIGURE 18. Speed curves of PD and hysteresis control.

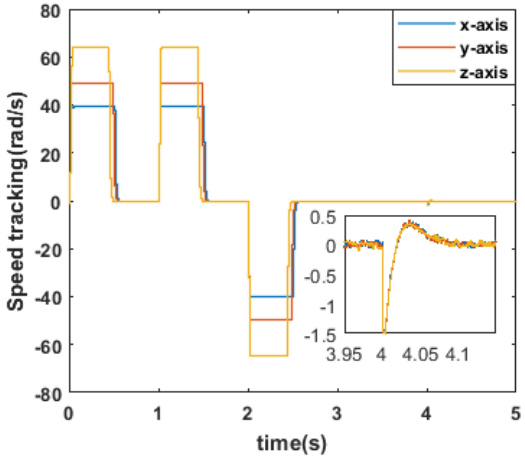

FIGURE 19. Speed curves of PCH and SMC control.

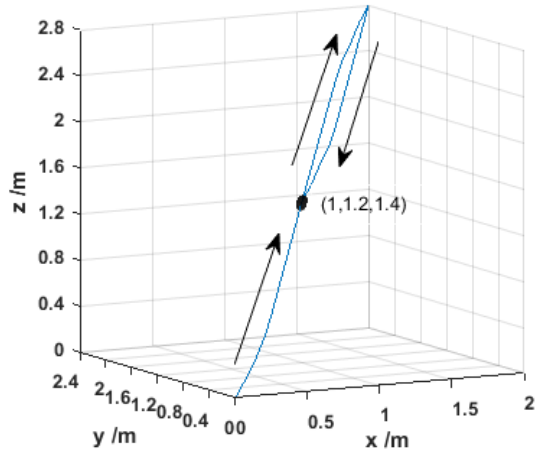

FIGURE 20. Space motion trajectory of PD and hysteresis control.

then at t=1s steps to (2m, 2.4m, 2.8m), at t=2s back to (1m, 1.2m, 1.4m). Fig.16 to Fig.19 show that PCH and SMC have better position and speed responses. Fig.20 and Fig.21 present that PCH and SMC strategies have smoother trajectories.

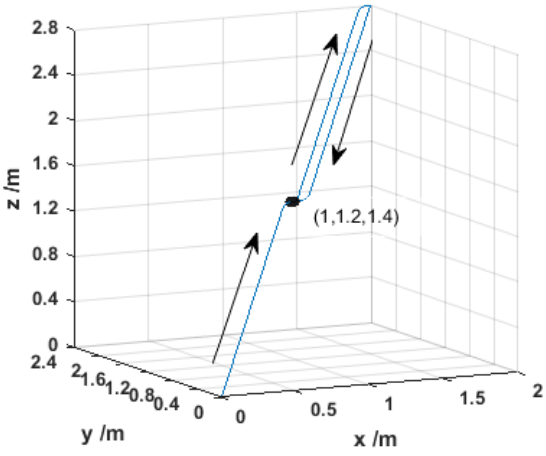

FIGURE 21. Space motion trajectory of PCH and SMC control.

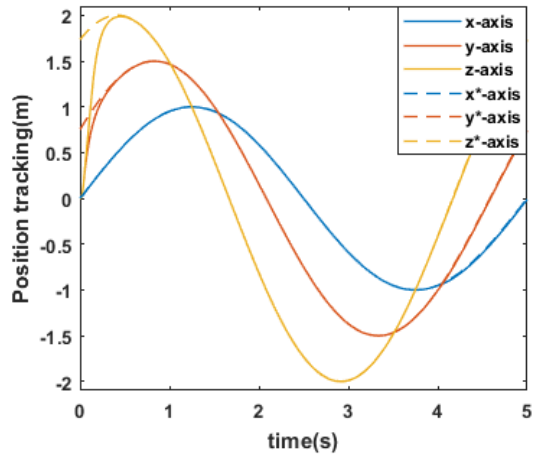

FIGURE 22. Position curves of PD and hysteresis control.

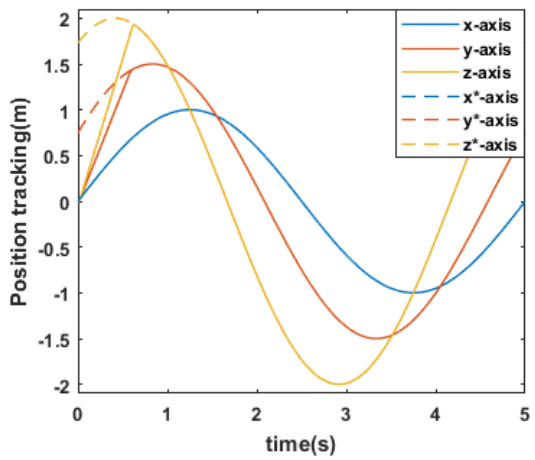

FIGURE 23. Position curves of PCH and SMC control.

Case 3: $x^* = \sin(\frac{2\pi}{5}t)rad, y^* = \sin(\frac{2\pi}{5}t + \frac{\pi}{6})rad, z^* = \sin(\frac{2\pi}{5}t + \frac{\pi}{3})rad$, which are periodic reference signals. Fig.22 to Fig.25 express the curves of position tracking,

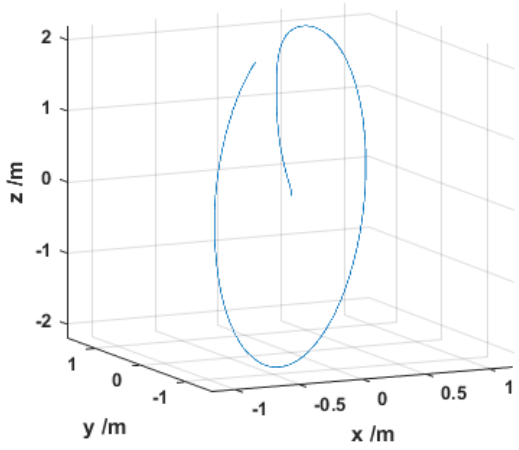

FIGURE 24. Space motion trajectory of PD and hysteresis control.

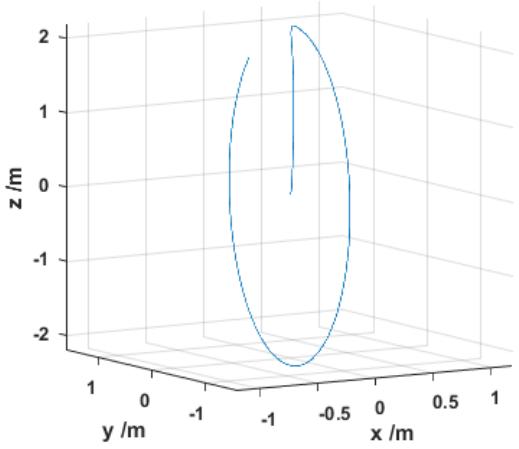

FIGURE 25. Space motion trajectory of PCH and SMC control.

space motion trajectory. From Fig.22 to Fig.23, the reference position is tracked by actual position, which shows that the PCH and SMC control strategies have excellent performance.

V. CONCLUSION

In view of gantry robot systems, a novel method of PCH and SMC is developed in this paper. The PCH controller is proposed by damping injection and energy-shaping. The desired equilibrium point is also determined. With the designed PCH controller, the gantry robot position control is achieved. For the drive systems of gantry robot, the DTC strategy based on SMC is applied to the IM drive systems, which reduces the torque and flux ripples. Moveover, the robot has good disturbance attenuation ability by introducing the load torque observer. Simulations show that the proposed control methods have good position tracking performance and fast speed responses under various conditions. In the future work, we will pay attention to the practical application of the proposed control strategy.

REFERENCES

[1] C. F. Baicu, C. D. Rahn, and D. M. Dawson, "Backstepping boundary control of flexible-link electrically driven gantry robots," *IEEE/ASME Trans. Mechatronics*, vol. 3, no. 1, pp. 60–66, Mar. 1998.

[2] S. Frikha, M. Djemel, and N. Derbel, "A new adaptive neuro-sliding mode control for gantry crane," *Int. J. Control, Automat. Syst.*, vol. 16, no. 2, pp. 559–565, Apr. 2018, doi: 10.1007/s12555-017-0070-x.

[3] Y. Zhang, P. Yan, and Z. Zhang, "High precision tracking control of a servo gantry with dynamic friction compensation," *ISA Trans.*, vol. 62, pp. 349–356, May 2016, doi: 10.1016/j.isatra.2016.02.006.

[4] W. Yin, L. Sun, M. Wang, and J. Liu, "Nonlinear state feedback position control for flexible joint robot with energy shaping," *Robot. Auton. Syst.*, vol. 99, no. 1, pp. 121–134, Jan. 2018, doi: 10.1016/j.robot.2017.10.007.

[5] V. Arakelian, "Gravity compensation in robotics," *Adv. Robot.*, vol. 30, no. 2, pp. 79–96, 2016.

[6] P. R. Ouyang, V. Pano, J. Tang, and W. H. Yue, "Position domain nonlinear PD control for contour tracking of robotic manipulator," *Robot. Comput.-Integr. Manuf.*, vol. 51, pp. 14–24, Jun. 2018, doi: 10.1016/j.rcim.2017.11.017.

[7] A. Arian, B. Danaei, H. Abdi, and S. Nahavandi, "Kinematic and dynamic analysis of the gantry-tau, a 3-DoF translational parallel manipulator," *Appl. Math. Model.*, vol. 51, pp. 217–231, Jun. 2017, doi: 10.1016/j.apm.2017.06.012.

[8] W. He, Y. Dong, and C. Sun, "Adaptive neural impedance control of a robotic manipulator with input saturation," *IEEE Trans. Syst., Man, Cybern. Syst.*, vol. 46, no. 3, pp. 334–344, Mar. 2016.

[9] W. He, Y. Chen, and Z. Yin, "Adaptive neural network control of an uncertain robot with full-state constraints," *IEEE Trans. Cybern.*, vol. 46, no. 3, pp. 620–629, Mar. 2016.

[10] R.-J. Wai, Y.-C. Huang, Z.-W. Yang, and C.-Y. Shih, "Adaptive fuzzy-neural-network velocity sensorless control for robot manipulator position tracking," *IET Control Theory Appl.*, vol. 4, pp. 1079–1093, Jun. 2010.

[11] L. Yu, S. Fei, J. Huang, and Y. Gao, "Trajectory switching control of robotic manipulators based on RBF neural networks," *Circuits Syst. Signal Process.*, vol. 33, no. 4, pp. 1119–1133, Apr. 2014.

[12] H. Yu, J. Yu, J. Liu, and Y. Wang, "Energy-shaping and L_2 gain disturbance attenuation control of induction motor," *Int. J. Innov. Comput. Inf. Control*, vol. 8, no. 7, pp. 5011–5024, Jul. 2012.

[13] H. Yu, J. Yu, J. Liu, and Q. Song, "Nonlinear control of induction motors based on state error PCH and energy-shaping principle," *Nonlinear Dyn.*, vol. 72, nos. 1–2, pp. 49–59, Apr. 2013.

[14] R. Ortega, F. Gomez-Estern, G. Blankenstein, and M. W. Spong, "Stabilization of a class of underactuated mechanical systems via interconnection and damping assignment," *IEEE Trans. Autom. Control*, vol. 47, no. 8, pp. 1218–1233, Aug. 2000.

[15] J. Chi, H. Yu, and J. Yu, "Hybrid tracking control of 2-DOF SCARA robot via port-controlled hamiltonian and backstepping," *IEEE Access*, vol. 6, pp. 17354–17360, 2018, doi: 10.1109/ACCESS.2018.2820681.

[16] I. M. Alsofyani and N. R. N. Idris, "Simple flux regulation for improving state estimation at very low and zero speed of a speed sensorless direct torque control of an induction motor," *IEEE Trans. Power Electron.*, vol. 31, no. 4, pp. 3027–3035, Apr. 2016.

[17] C. Lascu, I. Boldea, and F. Blaabjerg, "A modified direct torque control for induction motor sensorless drive," *IEEE Trans. Ind. Appl.*, vol. 36, no. 1, pp. 122–130, Jan. 2000.

[18] N. N. Venkataramana, A. Panda, and S. P. Singh, "A three-level fuzzy-2 DTC of induction motor drive using SVPWM," *IEEE Trans. Ind. Electron.*, vol. 63, no. 3, pp. 1467–1479, Mar. 2016.

[19] M. Habibullah, D. D.-C. Lu, D. Xiao, and M. F. Rahman, "A simplified finite-state predictive direct torque control for induction motor drive," *IEEE Trans. Ind. Electron.*, vol. 63, no. 6, pp. 3964–3975, Jun. 2016.

[20] A. Ammar, A. Benakcha, and A. Bourek, "Closed loop torque SVM-DTC based on robust super twisting speed controller for induction motor drive with efficiency optimization," *Int. J. Hydrogen Energy*, vol. 42, no. 28, pp. 17940–17952, Jul. 2017.

[21] C. M. R. Oliveira, M. L. Aguiar, J. R. B. A. Monteiro, W. C. A. Pereira, G. T. Paula, and T. E. P. Almeida, "PI control of induction motor using an integral sliding mode controller with anti-windup," *J. Control, Automat. Elect. Syst.*, vol. 8, no. 7, pp. 169–178, Apr. 2016.

[22] A. Ammar, A. Bourek, and A. Benakcha, "Sensorless SVM-direct torque control for induction motor drive using sliding mode observers," *J. Control, Automat. Elect. Syst.*, vol. 28, no. 2, pp. 189–201, Apr. 2017.

[23] A. Ammar, A. Bourek, and A. Benakcha, "Nonlinear SVM-DTC for induction motor drive using input-output feedback linearization and high order sliding mode control," *ISA Trans.*, vol. 67, pp. 428–442, Mar. 2017.

[24] H. Sudheer, S. F. Kodad, and B. Sarvesh, "Improvements in direct torque control of induction motor for wide range of speed operation using fuzzy logic," *J. Elect. Syst. Inf. Technol.*, to be published, doi: 10.1016/j.jesit.2016.12.015.
[25] R. Ortega, A. J. Van der Schaft, I. Mareels, and B. Maschke, "Putting energy back in control," *IEEE Control Syst. Mag*, vol. 21, no. 2, pp. 18–33, Apr. 2001.
[26] L. Yu, J. Huang, and S. Fei, "Sliding mode switching control of manipulators based on disturbance observer," *Circuits, Syst., Signal Process.*, vol. 36, no. 6, pp. 2574–2585, Jun. 2017.
[27] A. Mohammadi, M. Tavakoli, H. J. Marquez, and F. Hashemzadeh, "Nonlinear disturbance observer design for robotic manipulators," *Control Eng. Pract.*, vol. 21, no. 3, pp. 253–267, Mar. 2013.
[28] A. Rahoui, A. Bechouche, H. Seddiki, and D. O. Abdeslam, "Grid voltages estimation for three-phase PWM rectifiers control without AC voltage sensors," *IEEE Trans. Power Electron.*, vol. 33, no. 1, pp. 859–875, Jan. 2018.
[29] A. Ammar, A. Bourek, and A. Benakcha, "Robust SVM-direct torque control of induction motor based on sliding mode controller and sliding mode observer," *Frontiers Energy*, pp. 1–14, Jan. 2017, doi: 10.1007/s11708-017-0444-z.
[30] A. Djoudi, S. Bacha, H. Iman-Eini, and T. Rekioua, "Sliding mode control of DFIG powers in the case of unknown flux and rotor currents with reduced switching frequency," *Int. J. Elect. Power Energy Syst.*, vol. 96, pp. 347–356, Mar. 2018, doi: 10.1016/j.ijepes.2017.10.009.

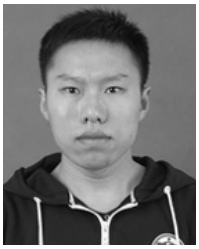

BINGKUN ZHAO received the B.Sc. degree in electrical engineering and automation from Shandong Jianzhu University, Jinan, China, in 2016. He is currently pursuing the M.Sc. degree in control science and engineering with Qingdao University, Qingdao, China. His research interests include robot control, electrical energy conversion, and motor control and applied nonlinear control.

HAISHENG YU received the B.S. degree in electrical automation from the Harbin University of Civil Engineering and Architecture in 1985, the M.S. degree in computer applications from Tsinghua University in 1988, and the Ph.D. degree in control science and engineering from Shandong University, China, in 2006. He is currently a Professor with the School of Automation Engineering, Qingdao University, China. His research interests include electrical energy conversion and motor control, applied nonlinear control, computer control, and intelligent systems.

JINPENG YU received the B.Sc. degree in automation from Qingdao University, Qingdao, China, in 2002, the M.Sc. degree in system engineering from Shandong University, Jinan, China, in 2006, and the Ph.D. degree from the Institute of Complexity Science, Qingdao University, in 2011. He is currently a Distinguished Professor with the School of Automation and Electrical Engineering, Qingdao University. His research interests include electrical energy conversion and motor control, applied nonlinear control, and intelligent systems. He was a recipient of the Shandong Province Taishan Scholar Special Project Fund and the Shandong Province Fund for Outstanding Young Scholars.

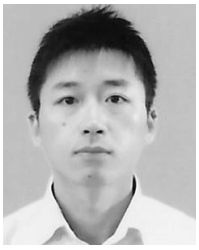

XUDONG LIU received the B.S. and M.S. degrees in automation from Qingdao University, Qingdao, China, in 2008 and 2011, respectively, and the Ph.D. degree in power electronics and electric drives from Shandong University, Jinan, China, in 2016. Since 2016, he has been with Qingdao University. His current research interests include new energy systems, power electronics, and motor drive.

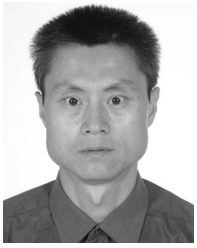

HERONG WU received the B.Sc. degree in automation from Qingdao University, Qingdao, China, in 1989. He is currently a senior Experimentalist with Qingdao University. His current research interests include computer control, programmable logic controller technology and application, process control, and motor control.